Chemistry & Biology
Article

Isolation and Purification of a New Kalimantacin/Batumin-Related Polyketide Antibiotic and Elucidation of Its Biosynthesis Gene Cluster

Wesley Mattheus,[1] Ling-Jie Gao,[2] Piet Herdewijn,[2] Bart Landuyt,[3] Jan Verhaegen,[4] Joleen Masschelein,[1] Guido Volckaert,[1] and Rob Lavigne[1,*]
[1]Laboratory of Gene Technology
[2]Interface Valorization Platform
[3]Animal Physiology and Neurobiology Section
[4]Experimental Laboratory Medicine
Katholieke Universiteit Leuven, Leuven B-3000, Belgium
*Correspondence: rob.lavigne@biw.kuleuven.be
DOI 10.1016/j.chembiol.2010.01.014

SUMMARY

Kal/bat, a polyketide, isolated to high purity (>95%) is characterized by strong and selective antibacterial activity against *Staphylococcus* species (minimum inhibitory concentration, 0.05 μg/mL), and no resistance was observed in strains already resistant to commonly used antibiotics. The *kal/bat* biosynthesis gene cluster was determined to a 62 kb genomic region of *Pseudomonas fluorescens* BCCM_ID9359. The *kal/bat* gene cluster consists of 16 open reading frames (ORF), encoding a hybrid PKS-NRPS system, extended with *trans*-acting tailoring functions. A full model for *kal/bat* biosynthesis is postulated and experimentally tested by gene inactivation, structural confirmation (using NMR spectroscopy), and complementation. The structural and microbiological study of biosynthetic *kal/bat* analogs revealed the importance of the carbamoyl group and 17-keto group for antibacterial activity. The mechanism of self-resistance lies within the production of an inactive intermediate, which is activated in a one-step enzymatic oxidation upon export. The genetic basis and biochemical elucidation of the biosynthesis pathway of this antibiotic will facilitate rational engineering for the design of novel structures with improved activities. This makes it a promising new therapeutic option to cope with multidrug-resistant clinical infections.

INTRODUCTION

In the antibiotic resistance age, which is marked by an increasing need for novel compounds (Von Nussbaum et al., 2006), secondary metabolites continue to play a major role in antibacterial drug discovery and development (Nathan, 2004). Their enormous structural complexity, linked with biological activity, forms an intrinsic advantage over synthetic compounds. Knowledge of their biosynthesis pathways substantially increases this advantage for the development of structural diversity through directed biosynthetic mutagenesis (Hopwood, 2004).

Polyketides and nonribosomal peptides represent two of the major classes of antibiotics, generated on multimodular enzymatic assembly lines. The modularity of the scaffold biosynthesis, together with the plurality of postassembly modifications by tailoring enzymes, offer prospects of creating novel antibiotics with optimized properties toward activity, production, and pharmacokinetics. The kalimantacin antibiotics were isolated from a fermentation broth of *Alcaligenes* species YL-02632S and display a strong antistaphylococcal effect (Kamigiri et al., 1996; Tokunaga et al., 1996) (Figure 1). The antibiotic batumin, which has the same molecular composition as kalimantacin A, was isolated from a culture liquid of *Pseudomonas batumici* and showed similar antimicrobial activity (Smirnov et al., 2000). To date, no batumin-resistant clinical staphylococcus isolates have been reported (Klochko et al., 2008). Batumin was previously shown to have only moderate activity against enterobacteria (*Salmonella*, *Bordetella*, *Escherichia*, and *Klebsiella* species) and no activity against micrococci and streptococci. Chemical- and UV-induced mutagenesis allowed the production of strains with 3.5-fold increased batumin production. During these experiments, histidine auxotrophy tended to be associated with loss of batumin production, hinting at a link between batumin biosynthesis and the histidine operon (Smirnov et al., 2000). The limited commercial availability and unsatisfying purity (<80%) of batumin hampers further research. Because the absolute configurations of the stereogenic carbon centers of all the above-mentioned compounds are not known, it is still unclear whether they are the same.

In this article, we present the isolation and purification of *kal/bat*, the sequence of the *kal/bat* gene cluster, and a model for its biosynthesis and self-resistance.

RESULTS

Microbiological Aspects and Purification/Characterization of the Antibiotic Compound

During the screening for novel antibiotics, a strain obtained from the BCCM/LMG Bacteria Collection (ID9359) displayed strong antibacterial activity against staphylococci. Sequence analysis of the ribosomal genes revealed that the strain belongs to the

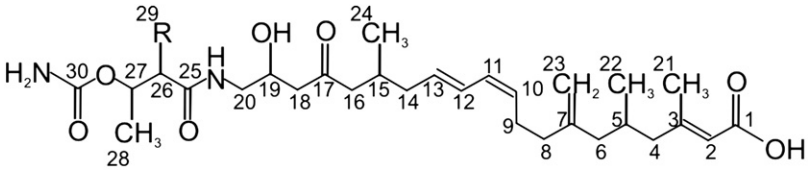

Kalimantacin A/Batumin (1) R= CH_3
Kalimantacin C (2) R= H

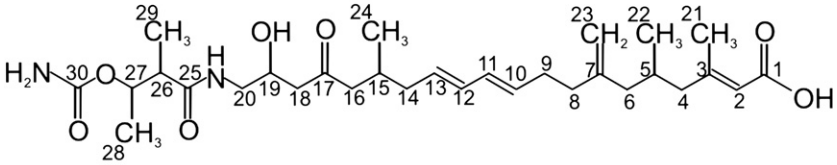

Kalimantacin B (3)

Figure 1. Structure of Kalimantacins and Batumin
The molecules have a linear polyketidal backbone with an incorporated glycine, multiple methyl branches, and a characteristic carbamoyl-group.

species *Pseudomonas fluorescens*. Fermentation experiments with *P. fluorescens* strain BCCM_ID9359 showed an optimal growth temperature of 28°C, whereas antibiotic production is significantly higher at 16°C. Antibiotic production followed the cell growth and reached a maximum after 48 hr (data not shown). HPLC analysis of crude extracts shows a peak with a retention time of 20.8 min (see Figure S1A available online); the extracts were purified and shown to have antibiotic activity on a bacterial lawn plate assay. HRMS revealed a molecular peak at [M + Na]/e = 571.3337, indicating a molecular formula of $C_{30}H_{48}N_2O_7Na$ (<1 ppm error) (Figure S1B), identical to those of kalimantacin A and batumin, which were independently isolated from *Alcaligenes* species strain YL-02632S and *P. batumici* fermentations, respectively (Kamigiri et al., 1996; Tokunaga et al., 1996; Smirnov et al., 2000). Large-scale purification by silica gel column chromatography yielded 35 mg/L of over 95% pure compound, allowing further structural and biological testing. ^1H and ^{13}C NMR spectra data verified the polyketide structure ((1); Figure 1) (Figures S1C and S1D). HPLC and HRMS analysis showed the remaining inpurity to be a secondary compound with a slightly reduced retention time of 20.2 min and a molecular peak at [M + Na]/e = 573.3501, indicating a molecular formula of $C_{30}H_{50}N_2O_7Na$ (Figures S1A and S2A). In ^1H NMR spectra, all of the typical peaks (olefinic proton and methyl protons) of the polyketide were present, which suggested that the product is a 17-keto reduction product. The new multipeak at 4.0 ppm indicated that an additional hydroxyl group was formed in the molecule. In ^{13}C NMR spectra, no peak corresponding to a keto group was observed, but a new peak at 66.1 ppm (typical chemical shift for secondary alcohol) appeared. These spectra data further proved the deduced structure (7). A detailed interpretation of ^1H and ^{13}C NMR spectra of 17-hydroxy *kal/bat* are shown in the Table S1 and Figures S2B and S2C.

The high yield and purity levels achieved for the active compound enabled accurate microbiological and chemical testing. Minimal inhibitory concentrations (MICs) of *kal/bat* were determined using NCCLS standards, confirming its rather selective activity against *Staphylococcus* species and, to a lesser extent, against enterobacteria (Table S2). During the course of screening, no *kal/bat*-resistant clinical *Staphylococcus* strains were discovered, and no resistance in strains already resistant to commonly used antibiotics was observed, hinting at a novel target or a strategy to bypass existing resistance.

Molecular Analysis of the Biosynthesis Pathway

Localization and identification of the kal/bat gene cluster

The biosynthesis gene cluster of this predicted polyketide was identified by random fragment sequencing and selection of similarity search results (BLASTx) related to polyketide biosynthesis gene products (Zazopoulos et al., 2003).

To verify the involvement of the predicted sequences in *kal/bat* biosynthesis, two encoding polyketide synthases (PKSs) (BatT1 and 2) and the one encoding a carbamoyl transferase (BatT3) were knocked out by integration of the pKnockout-G vector (Table S3B) (Yanisch-Perron et al., 1985). All three integration mutants (DisBatT1-3) displayed a complete loss of antibacterial activity against *S. aureus* ATCC6538 on plate bioassay, confirming their involvement in *kal/bat* biosynthesis (Figure 2).

To fully sequence the *kal/bat* biosynthesis cluster, a genomic BAC library was constructed and PCR-screened using the selected tags (primers are listed in Table S3C). Two BACs were sequenced by a combination of shotgun sequencing and primer walking, resulting in 114 kb and 113 kb of continuous sequence, respectively, and a combined total of 207 kb. Sequence data from the initial random genome sequencing (covering 25% of the cluster region) and the BAC sequencing revealed no discrepancies between both sets of sequences.

Flanking regions of the predicted cluster show strong homology (>85%) to the *P. fluorescens* Pf5 genome (Paulsen et al., 2005), whereas the *kal/bat* biosynthesis gene cluster appears to be of foreign origin. Gene prediction and annotation suggests an insertion through horizontal gene transfer of a region containing the *kal/bat* gene cluster between *P. fluorescens* Pf5 *PFL_3972* and *PFL_3969*. This correlates perfectly with a local decrease in G+C content from approximately 65% for the flanking regions to 56% for the fragment containing the gene cluster. The presence of a truncated transposase gene 3′ of the cluster further substantiates this assumption. On the basis of this assumption, we conclude that the *kal/bat* biosynthesis cluster is contained within the 77 kb fragment, encoding 28 predicted open reading frames (ORFs) in total (Figure 2; Table 1), most likely transcribed as a single operon.

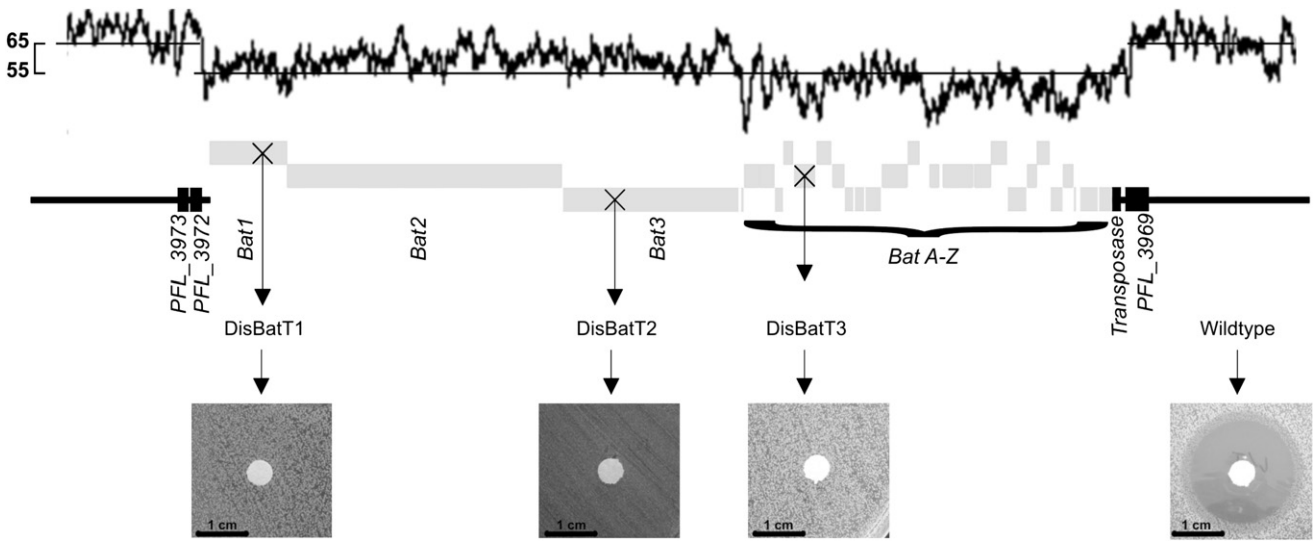

Figure 2. Organization of *kal/bat* Biosynthesis Cluster

ORFs are represented by grey (*kal/bat* biosynthesis) and black squares (flanking region)' predicted functions are listed in Table 1. Top of the figure shows G+C content, which significantly distinguishes the cluster from the flanking region. The positions of the three disruption mutants for the selected tags are marked by a cross. Down level shows the complete loss of antibacterial activity of the disruption mutants on a bacterial lawn plate bioassay, compared to the wild-type.

Genes encoding PKS/NRPS and tailoring enzymes

Sequence analysis revealed three large ORFs (*Bat1–Bat3*) encoding type I modular polyketide synthases, which cover 46 kb of the *kal/bat* cluster. Module and domain organization within Bat 1–3 were predicted on the basis of sequence similarity to known PKSs and are shown in Figure 3A. All *kal/bat* biosynthesis PKS modules lack AT domains, placing the *kal/bat* PKSs among the trans-AT PKSs. Two smaller ORFs (*BatH* and *BatJ*) encode discrete AT downstream of the modular ORFs, both of which contain the highly conserved active site GxSxG motif. Multiple alignment of BatH and BatJ and database ATs reveals conserved residues, correlated to substrate specificity, indicating that BatH is selective for acetyl-CoA, whereas BatJ is selective for malonyl-CoA (Yadav et al., 2003) (Figure S3A).

The building block specificity of the NRPS module is determined by the adenylation domain. Substrate specificity prediction with the support vector machine (SVM)–based program NRPSpredictor gives the glycine-code DILQLGLIWK with 100% identity, which is consistent with the structure prediction (Rausch et al., 2005).

Six potential β–ketoacyl reductase (KR) domains were identified and are all characterized by a Rossmann fold with the conserved NADPH-binding consensus and a catalytic S-Y-N triad (Reid et al., 2003). KR1-4,6 contain the LDD-loop characteristic for B-type KRs producing "R" hydroxyl groups, whereas this loop is missing in KR5, as seen in "S" hydroxyl-group producing A-type KRs (Caffrey, 2005; Reid et al., 2003) (Figure S3B).

Three potential dehydratase (DH) domains were identified and possess the conserved HxxxGxxxxP motif found in other DH domains (Donadio and Katz, 1992) (Figure S3C). The unusual position of DH2 exterior of a module has been observed in other PKSs, such as bacillaene and difficidin (Chen et al., 2006).

One potential methyltransferase (MT) domain with the conserved LExGxGxG motif (Kagan and Clarke, 1994) was identified and is located within PKS module 1 of Bat1. Because the final *kal/bat* structure contains five methyl branches, other enzymes in the tailoring region will be involved for their β-incorporation.

Sixteen potential acyl carrier proteins (ACPs) were identified, 15 as domains within the modular proteins and one as a separate ORF. The highly conserved signature motif LxDS is present in all ACPs, except for ACP10 (GVKS) and BatA (GANS) (Aparicio et al., 1996). The 4′-phospho-pantetheinylation of the essential serine residue is most likely performed by BatI, which shows homology to 4′-phospho-pantetheinyl transferases (Figure S3D). The same role as carrier in the NRPS module is performed by the peptidyl carrier protein (PCP). Although ACP and PCP domains are functionally similar, overall homology is limited, except for the 4′-phospho-pantetheine binding motif (GGDS for PCP1).

All predicted β-ketoacyl synthase (KS) domains contain the C-H-H catalytic triad, which is essential for the decarboxylative condensation. In KS7 only, which is positioned in between PKS module 6 and 7, the first histidine residue is missing, which might hint at the inactivity of KS7 (Figure S3E).

Condensation of the amino acid by the NRPS module is mediated by the condensation (C) domain with the HHxxxDG motif (Marahiel, 1997).

Finally, the polyketide biosynthesis is terminated by the thioesterase (TE) domain at the C-terminal end of Bat3. This domain should contain the characteristic GxSxG motif to catalyze the hydrophilic release of the mature polyketide chain from the PKS-complex (Konz and Marahiel, 1999). Interestingly, in the identified TE domain, the catalytic serine residue is replaced by a cysteine.

In addition to the three large multimodular PKS genes, 25 other putative ORFs have been identified within the gene cluster, some of which are likely to tailor the polyketidal scaffold produced by Bat1–3. *BatA–E* encode a β-methyl incorporation cassette

Table 1. Deduced Function of ORFs in the *kal/bat* Biosynthesis Gene Cluster

Gene	Product size (aa)	Proposed function	Protein homolog	Accession number	Protein similarity/identity (%/%)
Bat1	2239	PKS	onnB	AAV97870	41/56
Bat2	8013	PKS	BBR47_39870	YP_002773468	45/61
Bat3	5149	PKS	Bsubs1_010100009456	ZP_03591443	40/57
BatA	84	Acyl carrier protein	acpP2/sce3183	YP_001613822	60/74
BatB	405	Ketosynthase	sce3182	YP_001613821	66/77
BatC	420	3-hydroxy-3-methylglutaryl CoA synthase	BSU17150	NP_389595	73/84
BatD	258	Enoyl-CoA hydratase	sce3180	YP_001613819	59/77
BatE	250	Enoyl-CoA hydratase	Bsubs1_010100009446	ZP_03591441	67/84
BatF	582	Carbamoyl transferase	albXV	CAE52324	49/67
BatG	396	Trans-2-enoyl-CoA reductase	Vapar_4037	YP_002945917	61/78
BatH	321	Acyl transferase	sce3195	YP_001613834	48/62
BatI	265	4′-phosphopantetheinyl transferase	DeVSDRAFT_0201	ZP_02205079	50/66
BatJ	288	Acyl transferase	sce3195	YP_001613834	66/79
BatK	458	2-nitropropane dioxygenase	sce3184	YP_001613823	68/83
BatL	721	Methyltransferase	MICPUN_99875	XP_002501615	27/43
BatM	298	Short-chain dehydrogenase	BBR47_51660	YP_002774647	45/63
BatN	256	isobutylamine N-hydroxylase	CJA_3749	YP_001984200	95/221
BatO	103	Hypothetical protein	CJA_3749	YP_001984200	38/56
BatP	859	Aminotransferase	CJA_3750	YP_001984201	45/63
BatQ	469	Hypothetical protein	CJA_3751	YP_001984202	49/65
BatR	364	FAD dependent oxidoreductase	CJA_3752	YP_001984203	36/56
BatS	504	Choline/Carnitine o-acyltransferase	CJA_3754	YP_001984205	28/46
BatT	261	Short-chain dehydrogenase	CJA_3757	YP_001984208	51/65
BatU	341	Ferredoxin	Acry_1261	YP_001234391	31/47
BatV	365	Monooxygenase	Acry_1262	YP_001234392	36/53
BatW	273	Fatty acid desaturase	CfE428DRAFT_1380	ZP_03128215	33/53
BatX	85	Acyl carrier protein	BDU_706	YP_002222340	36/60
BatY	523	AMP-dependent synthetase	Npun_F3356	YP_001866726	45/65
BatZ	347	Fatty acid desaturase	MXAN_3495	YP_631689	32/49

functionally summarized in Table 1. Such cassettes have also been observed in biosynthesis clusters of mupirocin (El-Sayed et al., 2003), jamaicamide (Edwards et al., 2004), curacin (Chang et al., 2004), and pederin (Piel, 2002).

Other predicted tailoring genes include *BatF* (carbamoyl transferase), *BatK* (2-nitropropane dioxygenase), and *BatM* (secondary alcohol dehydrogenase), whereas the remaining genes cannot be directly linked to the *kal/bat* biosynthesis and may be involved in self-resistance, as discussed later.

Model for kal/bat biosynthesis and verification by knockout analysis

Because 12 building blocks are required to assemble the *kal/bat* backbone, the predicted modular constitution of Bat1–3 suggests that *kal/bat* biosynthesis proceeds collinearly, with each module performing only one chain extension per molecule. The domain organization and proposed *kal/bat* biosynthesis model are shown in Figure 3. To gain experimental insight into the *kal/bat* biosynthesis and to test the proposed model, specific in vivo gene inactivation experiments were performed using in frame deletions of all *kal/bat* tailoring ORFs, minimizing the risk of polar effects (Table 2). Phenotypes of the ORF-specific mutants were examined by plate bioassay, HPLC purification, FT-MS analysis, high-yield purification, and ^{1}H, ^{13}C NMR analysis and were functionally complemented *in trans*.

Deletion of *BatC* (HMG-CoA synthase) resulted in total loss of antibacterial activity against *S. aureus* ATCC6538. The HPLC profile revealed no detectable *kal/bat* or other related UV active compounds (Figure 4). As part of the β-methyl incorporation cassette, BatC is thought to introduce methyl-groups. This β-branch incorporation is a polarity reversal, compared with the S-adenosylmethionine–mediated methyl transfer seen in module 1. This system expands the possible methylation sites to both nucleophilic α-carbons and electrophilic β-carbons. Analogous to the in vitro proven bacillaene and myxovirescin pathways (Calderone et al., 2006) (Figure 3B), we propose that BatJ loads the freestanding ACP BatA with malonyl-CoA. BatB, with the missing cysteine of the C-H-H triad that is essential for condensation, decarboxylates malonyl-CoA-BatA to generate acetyl-CoA-BatA. The HMG-CoA synthase homolog, which is encoded by *BatC*, catalyzes the condensation between this acetate and the acetoacetate-like moieties generated by modules 5, 9, 10, and 11, respectively. Two members of the

enoyl-CoA hydratase family (BatD and BatE) contain the two consensus motifs essential for the oxyanion hole that stabilizes the enolate anions. These are hypothesized to catalyze the subsequent dehydration and decarboxylation (Gu et al., 2006). Knockout experiments of the corresponding HMG-CoA synthase homolog found in the mupirocin cluster resulted in the release of a truncated intermediate, mupirocin H (Wu et al., 2007). Interestingly, mutations in any of the other genes of the mupirocin β-methyl incorporation cassette gave the same phenotypic results (Wu et al., 2008). Similar to these results, the release of (4) (Figure 3A) is triggered, probably because the inactivity of BatC blocks the normal flux of metabolites along the multienzyme complex. As seen with mupirocin H, metabolite production levels might be significantly reduced, hampering the detection of intermediate (4). To verify that this phenotype is due to knocking out BatC, rather than polar effects, we amplified and inserted the *BatC* ORF into the broad-host-range IncQ expression vector pJH10. Expression *in trans* under control of the *tac* promoter fully restored wild-type *kal/bat* production.

Inactivation of BatF (carbamoyl transferase) led to a severely reduced antibacterial activity on plate bioassay. However, HPLC analysis performed on extracts of this mutant revealed production of a compound (25 mg/L) with a slightly shorter retention time of 20.6 min (Figure 4). Large-scale fermentation and purification of this compound ([M + Na]/e = 528.3287, $C_{29}H_{47}NO_6Na$ [<1 ppm error]) confirms the presence of the 27-descarbamoyl product ((6); Figure 4). Indeed, besides the chemical shifts and coupling constants for most of the typical peaks (olefinic protons and methyl protons) identical to those of *kal/bat*, only the chemical shift of 27-H shifted to up-field (from 4.89 ppm to 3.86 ppm). In addition, 29 peaks were observed in the ^{13}C- NMR spectra (corresponding to 29 carbons in the molecule), from which the peak corresponding to the carbamoyl group had disappeared. The chemical shift of C-27 shifted to up-field (from 73.5 ppm to 69.9 ppm), whereas C-28 shifted to down-field (from 17.9 ppm to 21.2 ppm). The chemical shifts of other carbons (far from C-27) are almost identical with that of *kal/bat*. These spectra data further confirmed the absence of a carbamoyl group ($CONH_2$) at C_{27} (Figure S4). This finding is consistent with the proposed role of BatF as O-carbamoyltransferase in the *kal/bat* biosynthesis. The detailed interpretation of ^1H and ^{13}C NMR spectra of 27-descarbamoyl *kal/bat* are shown in Table S1. Further examination of the antibacterial activity of 27-descarbamoyl *kal/bat* revealed an MIC of 0.512 μg/mL for *S. aureus* ATCC6538, which is eight times that of wild-type *kal/bat* (Table 2). This severely reduced activity of 27-descarbamoyl *kal/bat* confirms the importance of the carbamoyl-group for the antibacterial activity of *kal/bat*. As in the wild-type, a second minor product was isolated (2.3 mg/L) and was shown to be 17-hydroxy-27-descarbamoyl *kal/bat* ((8); Figure S5) by ^1H and ^{13}C NMR (Table S1). Complementation by expression of BatF *in trans* fully restored wild-type *kal/bat* production.

BatK shows similarity to the C-terminal portion of the *trans*-acting polyketide biosynthetic enzymes PksE and mmpIII (Chen et al., 2006; El-Sayed et al., 2003), found in bacillaene and mupirocin biosynthesis, respectively. This C-terminal moiety is predicted to encode a 2-nitropropane dioxygenase-like domain, associated with the N-terminal acyltransferase domain. Lomakin et al. (2007) reported strong structural similarity between the 2-nitropropane dioxygenase from *Pseudomonas aeruginosa* and the enoyl-reductase domain of the yeast fatty acid synthase. Bumpus et al. (2008) confirmed the trans-enoyl reductase activity of PksE in vitro. In frame deletion of *BatK* resulted in the total loss of antibacterial activity on plate bioassay, and no structurally related compounds were detected on HPLC (data not shown). On the basis of the homology with PksE, we hypothesize that BatK is responsible for the reduction of the olefin structure (5) during *kal/bat* biosynthesis. The inability to detect any unsaturated dihydro-*kal/bat* could be due to blockage of the normal flux of metabolites along the multienzyme complex or instability of this compound.

Deletion of the putative secondary alcohol dehydrogenase BatM resulted in a phenotype completely lacking antibacterial activity against *S. aureus* ATCC6538 on plate assay (Figure 4). HPLC, HRMS, and ^1H-, ^{13}C-NMR analysis on extracts showed the production of 17-hydroxy *kal/bat* (7) at yields (13 mg/L) significantly higher than in the wild-type (5 mg/L) and a complete lack of *kal/bat* production. Complementation by expression of BatM *in trans* fully restored wild-type *kal/bat* production. Further examination of the antibacterial activity of 17-hydroxy *kal/bat* (7) revealed an MIC of 4 μg/mL for *S. aureus* ATCC6538, showing that its activity is only 1.6% compared with that of *kal/bat* (Table 2). This strongly increased MIC value for 17-hydroxy *kal/bat* indicates the importance of the reoxydation of the hydroxygroup to a ketogroup at C_{17} for the antibacterial activity of *kal/bat* and suggests a role in self-resistance, as discussed later.

Both individual and multiple deletions of *BatG*, *BatL*, and *BatN-BatZ* (Table S3B) did not affect the antibacterial activity against *S. aureus* ATCC6538. HPLC and HRMS analysis confirmed the wild-type *kal/bat* production of all these knockouts (data not shown). This finding led us to the conclusion that the *kal/bat* biosynthesis cluster spans a 62 kb region that encodes 16 ORFs from *Bat1* to *BatM* and that is only part of the initially presumed 77 kb foreign fragment within the *P. fluorescens* strain.

General Discussion and Conclusions

The present study describes the isolation, purification, and characterization of a kalimantacin/batumin-related polyketide. The strain and procedure described here allowed us to isolate very pure *kal/bat* (>95%) in stable quantities of 35 mg/L for subsequent microbiological and chemical testing. Structural analysis revealed the same molecular structure as kalimantacin A and batumin, though the absolute stereochemical configuration of these compounds is still unknown. Antimicrobial spectra of *kal/bat* show results similar to those reported for kalimantacin and batumin (i.e., strong activity against staphylococci and moderate activity against enterobacteria). The apparent MIC of *kal/bat* for staphylococci was 0.05–0.10 μg/mL, which is slightly less than that observed for kalimantacin A and batumin. This finding might be explained by the high degree of purity achieved for the *kal/bat* isolation or by the possible difference in stereochemical configuration. Future crystallization studies on *kal/bat* will allow the confirmation of the chiral centers.

Biochemical characterization of the pathway using ORF-specific knockout experiments was consistent with the proposed biosynthesis model as a well-organized, collinear hybrid PKS-NRPS system, extended with *trans*-acting tailoring functions. The biosynthesis of the structurally related kalimantacin

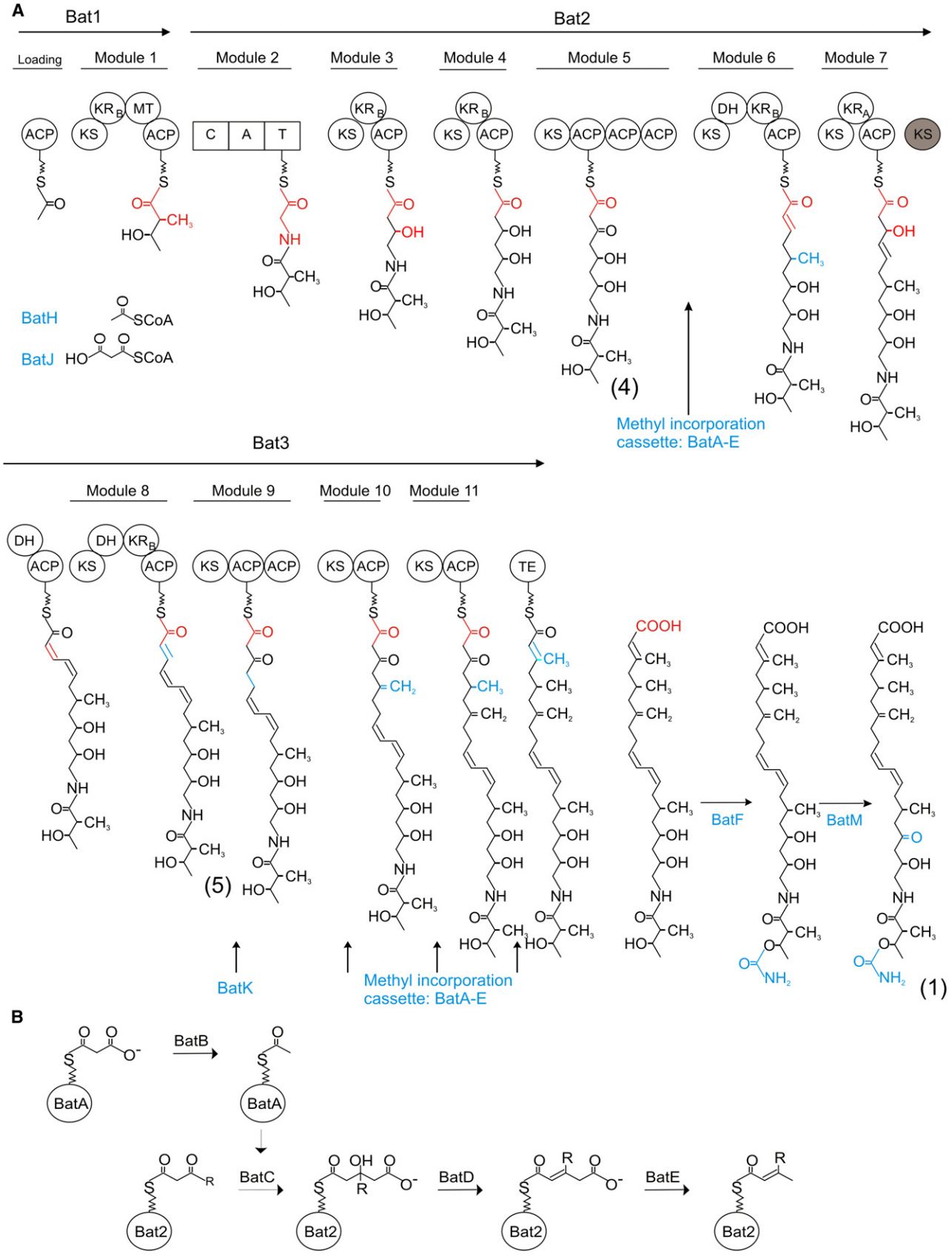
A
Bat1
Bat2
Loading
Module 1
Module 2
Module 3
Module 4
Module 5
Module 6
Module 7
BatH
BatJ
(4)
Methyl incorporation cassette: BatA-E
Bat3
Module 8
Module 9
Module 10
Module 11
(5)
BatK
Methyl incorporation cassette: BatA-E
BatF
BatM
(1)
B
BatB
BatA
BatC
BatD
BatE
Bat2

Table 2. Phenotypic Analysis of *P. fluorescens* Strain BCCM_ID9359 Deletion Knockouts

Strain	Function	Retention time (min)	Mol. mass	Structure	Yield (mg/L)	MIC (μg/mL)	Compl.
WT		20.8	548	$C_{30}H_{48}N_2O_7$	35	0.064	
		20.2	550	$C_{30}H_{50}N_2O_7$	5	4	
ΔbatC	HMG-CoA synthase	nd					+
ΔbatF	Carbamoyl transferase	20.6	505	$C_{29}H_{47}NO_6$	23	0.512	+
		20.1	507	$C_{29}H_{49}NO_6$	2.3	4	
ΔbatK	2-nitropropaan dioxygenase	nd					+
ΔbatM	Short-chain dehydrogenase	20.2	550	$C_{30}H_{50}N_2O_7$	13	4	+
ΔbatG, L, N-Y		20.8	548	$C_{30}H_{48}N_2O_7$	35	0.064	

nd, not detected.

antibiotics can be proposed to be similar to the *kal/bat* assembly: inactivity of the MT domain in module 1 would result in kalimantacin C ((2); Figure 1), whereas kalimantacin B ((3); Figure 1) would require an A-type to B-type KR domain substitution in module 7. During this work, there was no clue for a physical genomic linkage between *kal/bat* biosynthesis and the histidine operon, which was previously suggested in *P. batumici* (Smirnov et al., 2000).

Deletion of two of the tailoring enzymes (BatF and BatM) resulted in production of *kal/bat* analogs. Knockout strain ΔbatF produced 27-descarbamoyl *kal/bat* with an eight-fold reduced activity against *S. aureus.* In secondary metabolism, carbamoylation is often seen in bacterial nodulation factors that are produced upon induction by plant flavonoids (D'Haeze et al., 1999), but also in other natural antibiotics and antitumoral compounds (Steffensky et al., 2000; Coque et al., 1995; Galm et al., 2008). Studies on novobiocin, a bacterial type II topoisomerase DNA gyrase inhibitor, also highlighted the importance of the carbamoylation on activity. Removal of the carbamoyl-group resulted in a 100-fold reduction, whereas substitution by a 5-methylpyrrolyl acyl moiety, which is naturally produced as clorobiocin, is four times more active (Xu et al., 2004). In cefoxitine, a semisynthetic β-lactam antibiotic, the carbamoylation prevents in vivo deacetylation and subsequent inactivation (Queener et al., 1986). The availability of the mutant producing 27-descarbamoyl *kal/bat* can be an important first step to generate new *kal/bat*-analogs through combinatorial biosynthesis.

Testing of multidrug-resistant *S. aureus* strains revealed no cross-resistance, nor were any *kal/bat*-resistant clinical isolates found, hinting at a novel target. Interestingly, *P. fluorescens* pf5 showed an MIC of 1 μg/mL, whereas *P. fluorescens* strain BCCM_ID9359 is resistant to *kal/bat* (>128 μg/mL). To avoid suicide, *P. fluorescens* strain BCCM_ID9359 most likely developed a self-resistance mechanism, as seen in many other antibiotic-producing organisms (Cundliffe, 1989). This can be achieved by target modification, antibiotic modification, or an efficient efflux mechanism and is often encoded within the biosynthesis gene cluster. Knockout experiments on BatM revealed the importance of the reoxidation at C_{17} for the antibacterial activity of *kal/bat*. This one-step maturation converts an almost inactive precursor 17-hydroxy *kal/bat* into the fully active mature *kal/bat*. One may assume a regulation/resistance mechanism, given the seemingly illogical reduction/reoxidation null-operation as proposed by the model. The KR3 domain in module 4 first reduces the C_{17} keto-group and is later reoxidized by BatM. Indeed, together with the results of ΔBatM, there is no indication that KR3 of module 4 is inactive. Dot plot analysis revealed that KR3 is an exact copy of KR4 with conserved catalytic motifs. Second, an inactive KR3 would generate an unwanted acetoacetyl-like substrate susceptible to the β-methyl incorporation cassette. In addition, the intrinsic substrate specificity for β-hydroxy-substituted substrates of KS4 suggests an active KR3 (Nguyen et al., 2008). Export of an inactive intermediate and subsequent conversion to a toxic antibiotic has already been reported and is predominant through N-acetylation of amino groups or O-phosphorylation of hydroxyls (Cundliffe, 1989). The conversion to the active molecule is performed by a secreted deacetylase or phosphatase, respectively. Signal peptide analysis using SignalP-HMM predicted an N-terminal signal peptide in BatM, with 0.83 probability. Therefore, we propose that the inactive intermediate 17-hydroxy *kal/bat* is exported out of the cell for subsequent activation by the secreted BatM. Although this system is very similar to the previously mentioned systems, the important difference is that the inactive hydroxy-*kal/bat* is synthesized by the modular assembly line, rather than through the action of a separate enzyme. These individual antibiotic-inactivating enzymes (e.g., phosphotranferases and acetyltransferases) have shown to be an immediate source of resistance for pathogens through horizontal gene transfer, substantially increasing the rate of resistance development (D'Costa et al., 2006).

Figure 3. Proposed Model for *kal/bat* Biosynthesis

(A) Enzymatic domains of the PKS and NRPS are represented by circles and squares, respectively. Additions by each module are highlighted in red, and activities provided in *trans* are highlighted in blue. Initial loading was by BatH, and subsequent loadings were by BatJ. Reductive loop of module 6 introduces a *trans*-double bond (*E*), whereas split-module 7 produces a cis-double bond (*Z*), determined by the B-type and A-type KR domains, respectively. Module 8 shows a further reduction in *trans* of the olefinic intermediate by BatK. Final maturation of *kal/bat* was done through carbamoylation (BatF) and reoxidation (BatM).

(B) Mechanism of β-methyl incorporation (see explanation in text). Modules 5 and 9 contain an ACP triplet and douplet, respectively, which might help in channeling and docking intermediates to facilitate the β-methyl incorporation along with the elongation. AT, acyltransferase; KS, ketosynthase; ACP, acyl carrier protein; KR, ketoreductase ($_A$-type or $_B$-type, see text); DH, dehydrogenase; TE, thioesterase; C, condensation; A. adenylation; and T, thiolation.

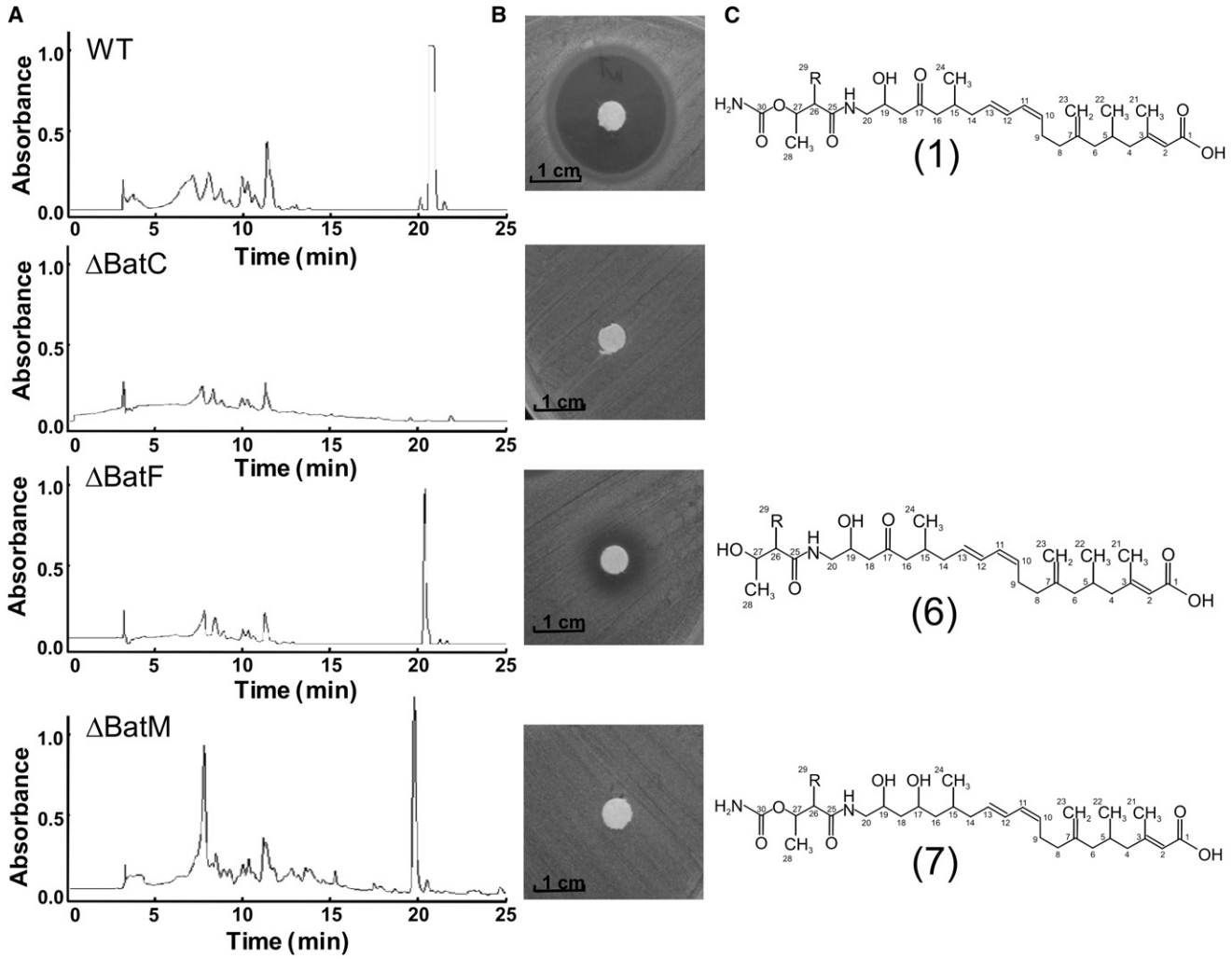

Figure 4. Phenotypic Analysis of *P. fluorescens* BCCM_ID9359 Knockouts

(A) HPLC profile of $CHCl_3$-extracts. Absorbance was measured at 228 nm. *kal*/*bat* and related analogs elute at approximately 20 min.

(B) Plate bioassay of purified *kal*/*bat* and analogs on *S. aureus* ATCC6538.

(C) HRMS and NMR spectroscopic confirmed structures of purified products.

Producing the inactive 17-hydroxy *kal*/*bat* by implementation in the multistep modular assembly circumvents this disadvantage.

Another possibility for the production of an inactive precursor is the "feed-forward" phenomenon—that is, an inactive precursor acts as a signal to prepare the producing organism for the later toxic levels of the antibiotic. Tahlan et al. (2008) showed that an antibiotically inactive precursor of actinorhodin derepressed transcription of the resistance pump gene at lower molar concentration than did actinorhodin itself, thus ensuring the full availability of the efflux system at the time the toxin is produced. The significantly reduced production of *kal*/*bat*-related compounds (13 mg/L of (7)) in ΔbatM, compared with wild-type (35 mg/L of (1)), and the fact that BatM most likely is active during export of *kal*/*bat* indicate a metabolite-regulated production.

Within the cluster, only gene products BatG (showing similarity to trans-enoyl-CoA reductases) and BatL (showing weak similarity to RNA methylases) appear to be nonessential for *kal*/*bat* production, making them plausible candidates to be involved in self-resistance.

The genetic basis and biochemical elucidation of the biosynthesis pathway of this novel type of antibiotic will facilitate rational engineering for the design of novel structures with improved activities. Indeed, a plurality of biosynthetic strategies combined in the *kal*/*bat* pathway was shown here. The backbone is assembled through a type 1 multimodular system with a combination of *trans*-acting "AT-less" PKS modules and a *cis*-acting NRPS module. Subsequent determination of the oxidation state happens through *cis*-acting catalytic domains or a *trans*-enoyl reductase involved in polyunsaturated fatty acid biosynthesis. Carbon branching is achieved on both nucleophilic α-carbons and electrophilic β-carbons through S-adenosylmethionine–mediated methyl transfer and an isoprenoid-like logic, respectively. This finding pinpoints once more that Nature's ingenuity for producing natural products is not restricted to classes of biosynthetic systems (Muller, 2004).

SIGNIFICANCE

In the antibiotic resistance age, which is marked by an increasing need for novel compounds, secondary metabolites continue to play a major role in antibacterial drug discovery and development. Polyketides represent a major class of antibiotics because they are amenable to rational antibiotic design by genetic modification within the modular biosynthesis operon. Our research focuses on a promising methicilin-resistant *Staphylococcus aureus* (a critical pathogen in hospital environments) antibiotic, synthesized by a plurality of polyketide biosynthetic strategies. Analysis of this molecule and its analogs shows its potential and amenability toward engineering with improved activity.

EXPERIMENTAL PROCEDURES

Bacterial Strains, Plasmids, and Culture Conditions

P. fluorescens strain BCCM_ID9359 was used as the wild-type *kal/bat* producer. The strain was grown at 28°C in tryptose-broth (Merck, Germany) for liquid cultivation and on tryptose-agar (Merck) for solid cultivation. *E. coli* Transformax™ EC100™ (Epicenter, US) was used for routine subcloning, plasmid preparations, and BAC cloning. *E. coli* S17-1 (Simon et al., 1983) was used for conjugal transfer of DNA into *P. fluorescens* strain BCCM_ID9359. *E. coli* strains were grown at 37°C in LB broth and LB agar (LB broth supplemented with 1.5% w/v agar). *S. aureus* ATCC6538 was used in bioassays to monitor *kal/bat* production. Media were supplemented with appropriate antibiotic concentrations as follows: ampicillin (100 mg/L), kanamycin (50 mg/L), triclosan (25 mg/L), chloramphenicol (15 mg/L), and tetracycline (15 mg/L). Plasmids used during this work are listed in Table S3A.

Production, Isolation, and Analysis of kal/bat

P. fluorescens strain BCCM_ID9359 was seeded in 250 mL of Tryptose broth in a 1 L Erlenmeyer flask and was incubated at 16°C on a rotary shaker (200 rpm) for 48 hr. To isolate *kal/bat*, the culture was adjusted to pH 10 with NaOH, and the cells were removed by centrifugation. After acidification with formic acid to pH 3, the supernatant was extracted with chloroform (2 × 250 mL) and was concentrated *in vacuo*. The extract was either used directly for HPLC analysis or was further purified by silica gel column chromatography. The HPLC analysis was performed on an Alltima C-18 column (5 μL, 250 × 4.6 mm; Alltech). The column was equilibrated with 100% solvent A (5% acetonitrile [ACN]; 0.1% TFA) and was developed with the following program: 0–1 min, 100% A; 1–30 min, a linear gradient from 100% A to 100% ACN; and 30–40 min, linear gradient from 100% ACN to 100% A at a flow rate of 1 mL/min and UV detection at 228 nm using a Shimadzu SPD-10A detector.

The silica gel column chromatography (20 × 250 mm; CH_2Cl_2/MeOH/HCOOH; 100/4/0.1 to 100/10/0.1) was used for large scale purification for subsequent NMR analysis and microbiological testing. MS analysis was performed on a Bruker Daltonics Apex-Qe FT mass spectrometer, and NMR was performed on a Bruker Ultrashield Avance instrument, operating at 600/300MHz for ^{1}H and 150/75MHz for ^{13}C nuclei in $CDCl_3$. The isolated yield for pure *kal/bat* from the wild-type *P. fluorescens* strain BCCM_ID9359 was 35 mg/L of culture medium.

Bioassay and MIC Determination

Kal/bat production was monitored by using the disk-diffusion method (Bauer et al., 1966). The Mueller-Hinton agar plate was uniformly inoculated with *S. aureus* ATCC6538, and a paper disk was impregnated with a culture sample or extrated product was placed on the agar surface. The size of the inhibition zone after 24 hr incubation is a relative measure for *kal/bat* production. MICs of *kal/bat* were determined using NCCLS standards (National Committee for Clinical Laboratory Standards, document M7-A5).

Library Construction and Screening of the kal/bat Biosynthesis Gene Cluster

A genomic random fragment library was constructed and sequenced. *P. fluorescens* strain BCCM_ID9359 genomic DNA was isolated, randomly sheared by ultrasonic vibration, and subsequently cloned in pUC19 using T4 DNA ligase (Promega). Transformation to *E. coli* Transformax™ EC100™ by electroporation yielded a library of over 10,000 clones with average insert size of 1 kb. Over 5000 clones were sequenced, resulting in a total of 3.5 Mb of raw data, which represent approximately 24% of the approximately 7 Mb *P. fluorescens* strain BCCM_ID9359 genome. Clones related to polyketide biosynthesis were identified by keyword searches of the batchBLAST analysis.

BAC genomic library construction of *P. fluorescens* strain BCCM_ID9359 was performed essentially as described by Osoegawa et al. (1998). High-molecular-weight DNA was isolated in plugs, partially digested with HindIII, and size selected by pulsed-field gel electrophoresis. Subsequent cloning in pIndigoBAC5 (Epicenter) and transformation to *E. coli* Transformax™ EC100™ were performed as recommended by the manufacturer and yielded a library of over 7000 clones with average inserts of 100 kb, resulting in a 34 times coverage of the genome. This library was screened by PCR for the presence of the *kal/bat* biosynthesis genes using the primers of the confirmed tags (Table S3C). PCRs were performed on cell cultures using GoTaq® DNA Polymerase (Promega) with an initial denaturation of 5 min for efficient bacterial lysis.

DNA Sequencing and Analysis

Selected BAC-clones were subcloned and sequenced by a combination of shotgun sequencing and primer walking. Sequencing reactions were run using Big Dye Terminator mix (Applied Biosystems), cleaned, and analyzed on an ABI 3130 genetic analyzer. Sequence assembly into contigs was performed using Sequencher 4.8 software (Gene Codes Corporation, USA). ORF predictions were made using comparative genomics approaches (tBLASTx) and the Genemark.hmm algorithm (Borodovsky et al., 2003).

Targeted Inactivation and Complementation

DNA transfer to *P. fluorescens* strain BCCM_ID9359 was performed through biparental mating with *E. coli* S17-1. A late exponential culture of *E. coli* with the relevant plasmid and *P. fluorescens* strain BCCM_ID9359 were mixed on a 0.45 μm sterile Millipore filter, placed on an LB-agar plate. After overnight incubation at 28°C, the mixture was resuspended in 1 mL of saline solution and spread on LB-agar plates supplemented with plasmid selective antibiotic and triclosan. Cointegrant clones were picked and incubated in tryptose broth without selection at 30°C overnight. Serial dilutions were spread on tryptose plates containing 5% sucrose, to select for vector excision. Deletion knockouts were screened by replica plating and PCR analysis. Clean-cut deletions were achieved by cloning two DNA fragments of approximately 300–500 bp flanking the targeted gene into the suicide vector pAKE604 (El-Sayed et al., 2001), whereas disruptions needed only 1 fragment into pKnockout-G suicide vector (Windgassen et al., 2000).

For the complementation experiments with pJH10, the same biparental mating procedure was used. Constructs prepared in this study are listed in Table S3B.

ACCESSION NUMBER

Sequencing data are accessible at GenBank under accession number GU479979.

SUPPLEMENTAL INFORMATION

Supplemental Information includes five figures and three tables and may be found with this article online at doi:10.1016/j.chembiol.2010.01.014.

ACKNOWLEDGMENTS

We thank Christopher M. Thomas for supplying vectors pAKE604 and pJH10. We also thank the Flemish Government for the financing of the mass spectrometry facility ProMeta.

Received: November 17, 2009
Revised: January 6, 2010
Accepted: January 14, 2010
Published: February 25, 2010

REFERENCES

Aparicio, J.F., Molanar, I., Schwecke, T., Koning, A., Haydock, S.F., Khaw, L.E., Staunton, J., and Leadlay, P.F. (1996). Organization of the biosynthetic gene cluster of rapamycin in *Streptomyces hygroscopicus*: analysis of the enzymatic domains in the modular polyketide synthase. Gene *169*, 9–16.

Bauer, A.W., Kirby, W.M., Sherris, J.C., and Turck, M. (1966). Antibiotic susceptibility testing by a standardized single disk method. Am. J. Clin. Pathol. *45*, 493–496.

Borodovsky, M., Mills, R., Besemer, J., and Lomsadze, A. (2003). Prokaryotic gene prediction using GeneMark and GeneMark.hmm. Curr. Protoc. Bioinformatics. *Chapter 4*, Unit 4.5.

Bumpus, S.B., Magarvey, N.A., Kelleher, N.L., Walsh, C.T., and Calderone, C.T. (2008). Polyunsaturated fatty-acid-like trans-enoyl reductases utilized in polyketide biosynthesis. J. Am. Chem. Soc. *130*, 11614–11616.

Caffrey, P. (2005). The stereochemistry of ketoreduction. Chem. Biol. *12*, 1060–1062.

Calderone, C.T., Kowtoniuk, W.E., Kelleher, N.L., Walsh, C.T., and Dorrestein, P.C. (2006). Convergence of isoprene and polyketide biosynthetic machinery: isoprenyl-S-carrier proteins in the pksX pathway of *Bacillus subtilis*. Proc. Natl. Acad. Sci. USA *103*, 8977–8982.

Chang, Z., Sitachitta, N., Rossi, J.V., Roberts, M.A., Flatt, P.M., Jia, J., Sherman, D.H., and Gerwick, W.H. (2004). Biosynthetic pathway and gene cluster analysis of curacin A, an antitubulin natural product from the tropical marine cyanobacterium *Lyngbya majuscula*. J. Nat. Prod. *67*, 1356–1367.

Chen, X.H., Vater, J., Piel, J., Franke, P., Scholz, R., Schneider, K., Koumoutsi, A., Hitzeroth, G., Grammel, N., Strittmatter, A.W., et al. (2006). Structural and functional characterization of three polyketide synthase gene clusters in *Bacillus amyloliquefaciens* FZB 42. J. Bacteriol. *188*, 4024–4036.

Coque, J.J., Pérez-Llarena, F.J., Enguita, F.J., Fuente, J.L., Martín, J.F., and Liras, P. (1995). Characterization of the cmcH genes of *Nocardia lactamdurans* and *Streptomyces clavuligerus* encoding a functional 3′-hydroxymethylcephem O-carbamoyltransferase for cephamycin biosynthesis. Gene *162*, 21–27.

Cundliffe, E. (1989). How antibiotic-producing organisms avoid suicide. Annu. Rev. Microbiol. *43*, 207–233.

D'Costa, V.M., McGrann, K.M., Hughes, D.W., and Wright, G.D. (2006). Sampling the antibiotic resistome. Science *311*, 374–377.

D'Haeze, W., Van Montagu, M., Promé, J.C., and Holsters, M. (1999). Carbamoylation of azorhizobial Nod factors is mediated by NodU. Mol. Plant Microbe Interact. *12*, 68–73.

Donadio, S., and Katz, L. (1992). Organization of the enzymatic domains in the multifunctional polyketide synthase involved in erythromycin formation in *Saccharopolyspora erythraea*. Gene *111*, 51–60.

Edwards, D.J., Marquez, B.L., Nogle, L.M., McPhail, K., Goeger, D.E., Roberts, M.A., and Gerwick, W.H. (2004). Structure and biosynthesis of the jamaicamides, new mixed polyketide-peptide neurotoxins from the marine cyanobacterium *Lyngbya majuscula*. Chem. Biol. *11*, 817–833.

El-Sayed, A.K., Hothersall, J., and Thomas, C.M. (2001). Quorum-sensing-dependent regulation of biosynthesis of the polyketide antibiotic mupirocin in *Pseudomonas fluorescens* NCIMB 10586. Microbiology *147*, 2127–2139.

El-Sayed, A.K., Hothersall, J., Cooper, S.M., Stephens, E., Simpson, T.J., and Thomas, C.M. (2003). Characterization of the mupirocin biosynthesis gene cluster from *Pseudomonas fluorescens* NCIMB 10586. Chem. Biol. *10*, 419–430.

Galm, U., Wang, L., Wendt-Pienkowski, E., Yang, R., Liu, W., Tao, M., Coughlin, J.M., and Shen, B. (2008). In vivo manipulation of the bleomycin biosynthetic gene cluster in *Streptomyces verticillus* ATCC15003 revealing new insights into its biosynthetic pathway. J. Biol. Chem. *283*, 28236–28245.

Gu, L., Jia, J., Liu, H., Håkansson, K., Gerwick, W.H., and Sherman, D.H. (2006). Metabolic coupling of dehydration and decarboxylation in the curacin A pathway: functional identification of a mechanistically diverse enzyme pair. J. Am. Chem. Soc. *128*, 9014–9015.

Hopwood, D.A. (2004). Cracking the polyketide code. PLoS Biol. *2*, e35.

Kagan, R.M., and Clarke, S. (1994). Widespread occurrence of three sequence motifs in diverse S-adenosylmethionine-dependent methyltransferases suggests a common structure for these enzymes. Arch. Biochem. Biophys. *310*, 417–427.

Kamigiri, K., Suzuki, Y., Shibazaki, M., Morioka, M., Suzuki, K., Tokunaga, T., Setiawan, B., and Rantiatmodjo, R.M. (1996). Kalimantacins A, B and C, novel antibiotics from *Alcaligenes* sp. YL-02632S. I. Taxonomy, fermentation, isolation and biological properties. J. Antibiot. (Tokyo) *49*, 136–139.

Klochko, V.V., Kiprianova, E.A., Churkina, L.N., and Avdeeva, L.V. (2008). Antimicrobial spectrum of antibiotic batumin. Mikrobiol. Z. *70*, 41–46.

Konz, D., and Marahiel, M.A. (1999). How do peptide synthetases generate structural diversity? Chem. Biol. *6*, R39–R48.

Lomakin, I.B., Xiong, Y., and Steitz, T.A. (2007). The crystal structure of yeast fatty acid synthase, a cellular machine with eight active sites working together. Cell *129*, 319–332.

Marahiel, M.A. (1997). Protein templates for the biosynthesis of peptide antibiotics. Chem. Biol. *4*, 561–567.

Muller, R. (2004). Don't classify polyketide synthases. Chem. Biol. *11*, 4–6.

Nathan, C. (2004). Antibiotics at the crossroads. Nature *431*, 899–902.

Nguyen, T., Ishida, K., Jenke-Kodama, H., Dittmann, E., Gurgui, C., Hochmuth, T., Taudien, S., Platzer, M., Hertweck, C., and Piel, J. (2008). Exploiting the mosaic structure of trans-acyltransferase polyketide synthases for natural product discovery and pathway dissection. Nat. Biotechnol. *26*, 225–233.

Osoegawa, K., Woon, P.Y., Zhao, B., Frengen, E., Tateno, M., Catanese, J.J., and de Jong, P.J. (1998). An improved approach for construction of bacterial artificial chromosome libraries. Genomics *52*, 1–8.

Paulsen, I.T., Press, C.M., Ravel, J., Kobayashi, D.Y., Myers, G.S., Mavrodi, D.V., DeBoy, R.T., Seshadri, R., Ren, Q., Madupu, R., et al. (2005). Complete genome sequence of the plant commensal *Pseudomonas fluorescens* Pf-5. Nat. Biotechnol. *23*, 873–878.

Piel, J. (2002). A polyketide synthase-peptide synthetase gene cluster from an uncultured bacterial symbiont of Paederus beetles. Proc. Natl. Acad. Sci. USA *99*, 14002–14007.

Queener, S.F., Webber, J.A., and Queener, S.W. (1986). Beta-Lactam Antibiotics for Clinical Use (New York: Marcel Dekker).

Rausch, C., Weber, T., Kohlbacher, O., Wohlleben, W., and Huson, D.H. (2005). Specificity prediction of adenylation domains in nonribosomal peptide synthetases (NRPS) using transductive support vector machines (TSVMs). Nucleic Acids Res. *33*, 5799–5808.

Reid, R., Piagentini, M., Rodriguez, E., Ashley, G., Viswanathan, N., Carney, J., Santi, D.V., Hutchinson, C.R., and McDaniel, R. (2003). A model of structure and catalysis for ketoreductase domains in modular polyketide synthases. Biochemistry *42*, 72–79.

Simon, R., Priefer, U., and Pühler, A. (1983). A broad host range mobilization system for in vivo genetic engineering: transposon mutagenesis in gram negative bacteria. Nat. Biotechnol. *1*, 784–791.

Smirnov, V.V., Churkina, L.N., Perepnikhatka, V.I., Mukvich, N.S., Garagulia, A.D., Kiprianova, E.A., Kravets, A.N., and Dovzhenko, S.A. (2000). Isolation of highly active strain producing the antistaphylococcal antibiotic batumin. Prikl. Biokhim. Mikrobiol. *36*, 55–58.

Steffensky, M., Mühlenweg, A., Wang, Z.X., Li, S.M., and Heide, L. (2000). Identification of the novobiocin biosynthetic gene cluster of *Streptomyces spheroides* NCIB 11891. Antimicrob. Agents Chemother. *44*, 1214–1222.

Tahlan, K., Yu, Z., Xu, Y., Davidson, A.R., and Nodwell, J.R. (2008). Ligand recognition by ActR, a TetR-like regulator of actinorhodin export. J. Mol. Biol. *383*, 753–761.

Tokunaga, T., Kamigiri, K., Orita, M., Nishikawa, T., Shimizu, M., and Kaniwa, H. (1996). Kalimantacin A, B, and C, novel antibiotics produced by *Alcaligenes*

sp. YL-02632S. II. Physico-chemical properties and structure elucidation. J. Antibiot. (Tokyo) *49*, 140–144.

Von Nussbaum, F., Brands, M., Hinzen, B., Weigand, S., and Häbich, D. (2006). Antibacterial natural products in medicinal chemistry—exodus or revival? Angew. Chem. Int. Ed. Engl. *45*, 5072–5129.

Windgassen, M., Urban, A., and Jaeger, K.-E. (2000). Rapid gene inactivation in *Pseudomonas aeruginosa*. FEMS Microbiol. Lett. *193*, 201–205.

Wu, J., Cooper, S.M., Cox, R.J., Crosby, J., Crump, M.P., Hothersall, J., Simpson, T.J., Thomas, C.M., and Willis, C.L. (2007). Mupirocin H, a novel metabolite resulting from mutation of the HMG-CoA synthase analogue, mupH in *Pseudomonas fluorescens*. Chem. Commun. (Camb.) *20*, 2040–2042.

Wu, J., Hothersall, J., Mazzetti, C., O'Connell, Y., Shields, J.A., Rahman, A.S., Cox, R.J., Crosby, J., Simpson, T.J., Thomas, C.M., and Willis, C.L. (2008). In vivo mutational analysis of the mupirocin gene cluster reveals labile points in the biosynthetic pathway: the "leaky hosepipe" mechanism. ChemBioChem *9*, 1500–1508.

Xu, H., Heide, L., and Li, S.M. (2004). New aminocoumarin antibiotics formed by a combined mutational and chemoenzymatic approach utilizing the carbamoyltransferase NovN. Chem. Biol. *11*, 655–662.

Yadav, G., Gokhale, R.S., and Mohanty, D. (2003). Computational approach for prediction of domain organization and substrate specificity of modular polyketide synthases. J. Mol. Biol. *328*, 335–363.

Yanisch-Perron, C., Vieira, J., and Messing, J. (1985). Improved M13 phage cloning vectors and host strains: nucleotide sequences of the M13mp18 and pUC19 vectors. Gene *33*, 103–119.

Zazopoulos, E., Huang, K., Staffa, A., Liu, W., Bachmann, B.O., Nonaka, K., Ahlert, J., Thorson, J.S., Shen, B., and Farnet, C.M. (2003). A genomics-guided approach for discovering and expressing cryptic metabolic pathways. Nat. Biotechnol. *21*, 187–190.